Bioactive Materials 5 (2020) 398–409

Contents lists available at ScienceDirect

Bioactive Materials

journal homepage: http://www.keaipublishing.com/biomat

Biodegradation behavior of micro-arc oxidation coating on magnesium alloy-from a protein perspective

Zhao-Qi Zhang[a,b], Li Wang[b], Mei-Qi Zeng[a], Rong-Chang Zeng[a,c,*], M. Bobby Kannan[d], Cun-Guo Lin[b,**], Yu-Feng Zheng[e]

[a] Corrosion Laboratory for Light Metals, College of Material Science and Engineering, Shandong University of Science and Technology, Qingdao, 266590, China
[b] State Key Laboratory for Marine Corrosion and Protection, Luoyang Ship Material Research Institute, Qingdao, 266101, China
[c] School of Materials Science and Engineering, Zhengzhou University, Zhengzhou, 450002, China
[d] Biomaterials and Engineering Materials (BEM) Laboratory, College of Science, Technology and Engineering, James Cook University, Townsville, 4811, Australia
[e] State Key Laboratory for Turbulence and Complex Systems and Department of Materials Science and Engineering, College of Engineering, Peking University, Beijing, 100871, China

ARTICLE INFO

Keywords:
Magnesium alloy
Protein
Degradation
Micro-arc oxidation
Biocompatibility

ABSTRACT

Protein exerts a critical influence on the degradation behavior of absorbable magnesium (Mg)-based implants. However, the interaction mechanism between protein and a micro-arc oxidation (MAO) coating on Mg alloys remains unclear. Hereby, a MAO coating was fabricated on AZ31 Mg alloy. And its degradation behavior in phosphate buffer saline (PBS) containing bovine serum albumin (BSA) was investigated and compared with that of the uncoated alloy. Surface morphologies and chemical compositions were studied using Field-emission scanning electron microscope (FE-SEM), Fourier transform infrared spectrophotometer (FT-IR) and X-ray diffraction (XRD). The degradation behavior of the bare Mg alloy and its MAO coating was studied through electrochemical and hydrogen evolution tests. Cytotoxicity assay was applied to evaluate the biocompatibility of Mg alloy substrate and MAO coating. Results indicated that the presence of BSA decreased the degradation rate of Mg alloy substrate because BSA ($RCH(NH_2)COO^-$) molecules combined with Mg^{2+} ions to form $(RCH(NH_2)COO)_2Mg$ and thus inhibited the dissolution of $Mg(OH)_2$ by impeding the attack of Cl^- ions. In the case of MAO coated Mg alloy, the adsorption of BSA on MAO coating and the formation of $(RCH(NH_2)COO)_2Mg$ exhibited a synergistic effect and enhanced the corrosion resistance of the coated alloy significantly. Furthermore, cell bioactive assay suggested that the MAO coating had good viability for MG63 cells due to its high surface area.

1. Introduction

Today, magnesium (Mg) and its alloys are implantable materials due to their superior biocompatibility and biodegradable properties [1–5]. However, Mg and its alloys degrade too fast due to their lower electrochemical potentials [6,7], limiting their use as implants. Hence, various surface modifications have been employed to control the degradation rate of implantable Mg and its alloy. The surface modifications include layered double hydroxides (LDH) [8,9], calcium phosphates and Hydroxyapatite (HA) [10–12], montmorillonite [13], micro-arc oxidation (MAO) [14–16], and layer-by-layer self-assembly (LbL) [17,18] together with polymeric coatings (e.g. polylactic acid and silane coating) [19–21].

MAO coating has been widely utilized on Mg and its alloys [22]. By a MAO process, a hard and porous ceramic coating is created on Mg substrate [23–25]. The coating is formed through a chemical conversion of Mg substrate into its oxides, which grows both outwards and inwards. Zheng et al. [26] studied MAO coating on Mg–Ca alloys by altering the applied voltages (300, 360 and 400 V). The results indicated that MAO coating obtained at 360 V exhibited the best corrosion resistance and all MAO coatings improved the cell adhesion. Yao et al. [27] found that incorporating P and Ca into a MAO-treated AZ91D alloy enhanced its corrosion-resistant performance. In other words, MAO coatings have shown favorable corrosion resistance, good

Peer review under responsibility of KeAi Communications Co., Ltd.
* Corresponding author. Corrosion Laboratory for Light Metals, College of Material Science and Engineering, Shandong University of Science and Technology, Qingdao, 266590, China.
** Corresponding author. State Key Laboratory for Marine Corrosion and Protection, Luoyang Ship Material Research Institute, Qingdao, 266101, China.
E-mail addresses: rczeng@foxmail.com (R.-C. Zeng), lincg@sunrui.net (C.-G. Lin).

https://doi.org/10.1016/j.bioactmat.2020.03.005
Received 7 February 2020; Received in revised form 6 March 2020; Accepted 6 March 2020
Available online 30 March 2020

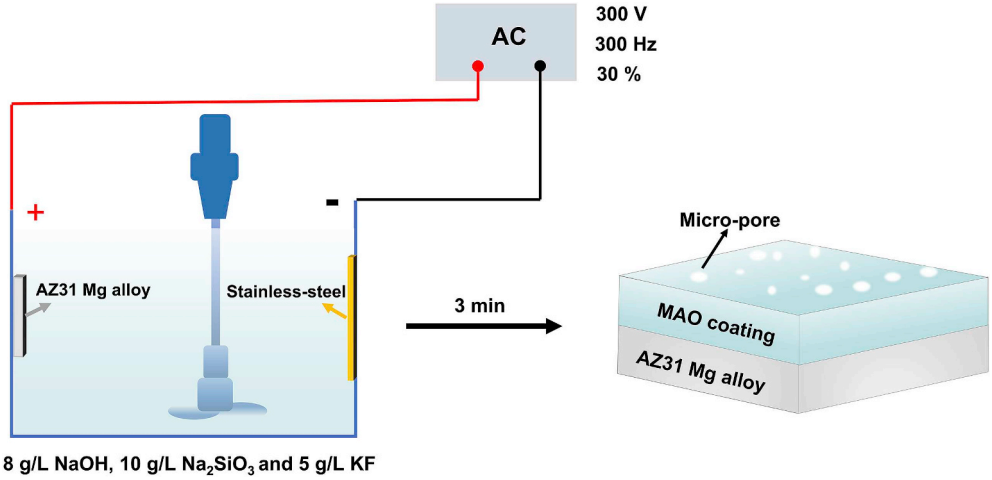

Fig. 1. Schematic diagram of the preparation of MAO coating.

biocompatibility and excellent adhesion to Mg substrate [26,28,29].

Typically, the physiological solution (i.e. blood plasma) in human body contains both inorganic ions and organic components. The inorganic ions contain cations such as Ca^{2+}, Mg^{2+}, Na^{+} and K^{+}, and anions such as HCO_3^{-}, Cl^{-}, $H_2PO_4^{-}$, HPO_4^{2-} and SO_4^{2-} [30]; whereas, the organic species include glucose, amino acids and protein (e.g. albumin) and so on. Our recent investigations showed that pure Mg exhibits different corrosion behaviors in Hank's and NaCl solutions with or without organic species [31]. The presence of glucose in NaCl solution accelerates corrosion rate of pure Mg due to the formation of gluconic acid, which attacks the oxides of the metal and promotes the absorption of Cl^{-} ions on the Mg surface. Interestingly, pure Mg possesses a better corrosion resistance in Hank's solution than in saline or 0.9 wt% NaCl solution with the presence of glucose, which can be attributed to the fact that glucose coordinates Ca^{2+} ions in Hank's solution and thus improves the formation of Ca–P compounds on pure Mg surface. The presence of both glucose and amino acids in 0.9 wt% NaCl solution gives rise to accelerated corrosion of the pure Mg samples due to the formation of schiff's base (-C═N-) [32]. Similar results have been reported for Mg–Ca and AZ31 Mg alloys [1,6]. Cui et al. [6] reported that glucose accelerates the corrosion rate of Mg–1.35Ca alloy in saline solution through dissolving the $Mg(OH)_2$ film. Li et al. [1] found that the lower concentration (1 g/L) of glucose can inhibit the corrosion behavior of AZ31 Mg alloy owing to complex formation with Mg^{2+} ions, thereby preventing the contact of Cl^{-} ions with the metal surface. However, higher content (2 and 3 g/L) of glucose can increase the corrosion rate due to the transformation of glucose into gluconic acid, thus promoting the absorption of Cl^{-} ions on to the surface.

Proteins also play an important role in the degradation behavior of Mg and its alloys. However, there is no consensus over the influence of proteins on the degradation of Mg and its alloys. Liu et al. [33] reported that protein retards the degradation of Mg–Ca alloy in PBS solution due to the synergistic effect of OH^{-} ions and negatively charged albumin molecules that can inhibit the attack from aggressive Cl^{-} ions. Yamamoto et al. [34] suggested that the adsorption of protein and the formation of insoluble salts reduce the degradation of Mg substrate; whereas amino acids promote the degradation of pure Mg. Interestingly, Wang et al. [35] reported that the adsorption of albumin prohibits the corrosion of Mg alloy M1A during the initial immersion period. However, the presence of albumin accelerates the dissolution of Mg alloy with the chelation effect in the later stage. Hence, it is critical to further investigate the in vitro degradation mechanism of the Mg alloy and its MAO coating in protein environment.

This study aims to investigate the interaction mechanism between proteins and MAO coated Mg alloys, and to clarify the biodegradation mechanism of MAO coating from a protein perspective. Moreover, the biocompatibility of Mg alloys and its MAO coating was evaluated.

2. Experiment

2.1. Materials and chemicals

The as-extruded Mg alloy AZ31 sheets (nominal compositions: Al 2.5–3.0 wt%, Zn 0.7–1.3 wt%, Mn > 0.20 wt% and the balance Mg) were obtained from Shandong Yinguang Yuyuan Light Metal Precise Forming Co. Ltd. China. Bovine serum albumin (BSA) was procured from Sinopharm Chemical Reagent Co. Ltd. China. The AZ31 Mg substrate was cut into a dimension of 20 × 20 × 5 mm, and ground with 1200 grit SiC paper. Before coating, the AZ31 Mg sheet was cleaned with distilled water and ethanol, and dried in warm air.

2.2. Coating preparation

The pre-treated Mg AZ31 sheet was anodized using a home-made MAO equipment. The device consisted of a power supply unit controlled by a single chip micyoco, a stainless-steel plate as cathode and a cooling system (Fig. 1). MAO coating was prepared with an AC power supply with a duty cycle of 30%, a constant voltage of 300 V and a fixed frequency of 300 Hz for 3 min. The electrolyte contained 8 g/L of NaOH, 10 g/L of Na_2SiO_3 and 5 g/L of KF [36]. In this experiment, the MAO coating was formed on the Mg AZ31 substrate through constant voltage. The voltage was increased successively (0 V, 150 V, 180 V, 220 V, 250 V, 280 V and 300 V) until 300 V in the preparation process, and the preparation time was controlled at 3 min. Then, the prepared MAO coating was taken out, cleaned with distilled water, and dried in warm air before surface characterization.

2.3. Surface analysis

Field-emission scanning electronic microscope (FE-SEM, Hitachi S-4800, Japan) was employed to study the surface and cross-sections morphologies of the samples; and the elemental compositions were detected through an energy dispersive X-ray spectrometer (EDS). Crystal structures of the coatings were investigated through X-ray diffractometer (XRD, Rigaku D/MAX 2500 PC, Japan) with Cu Kα radiation, and diffraction pattern was generated between 2θ values of 5–80°. The chemical compositions of the degradation products were analyzed via Fourier transform infrared spectrophotometer (FT-IR, Nicolet 380, Thermo Fisher Scientific, USA) in the regular wave-numbers range (600–3800 cm^{-1}). X-ray photoelectron spectrometer (XPS, ESCALAB 250 Xi, Thermo Fisher Scientific, USA) was used to investigate the chemical states of specimens after immersion, and the XPS spectrum

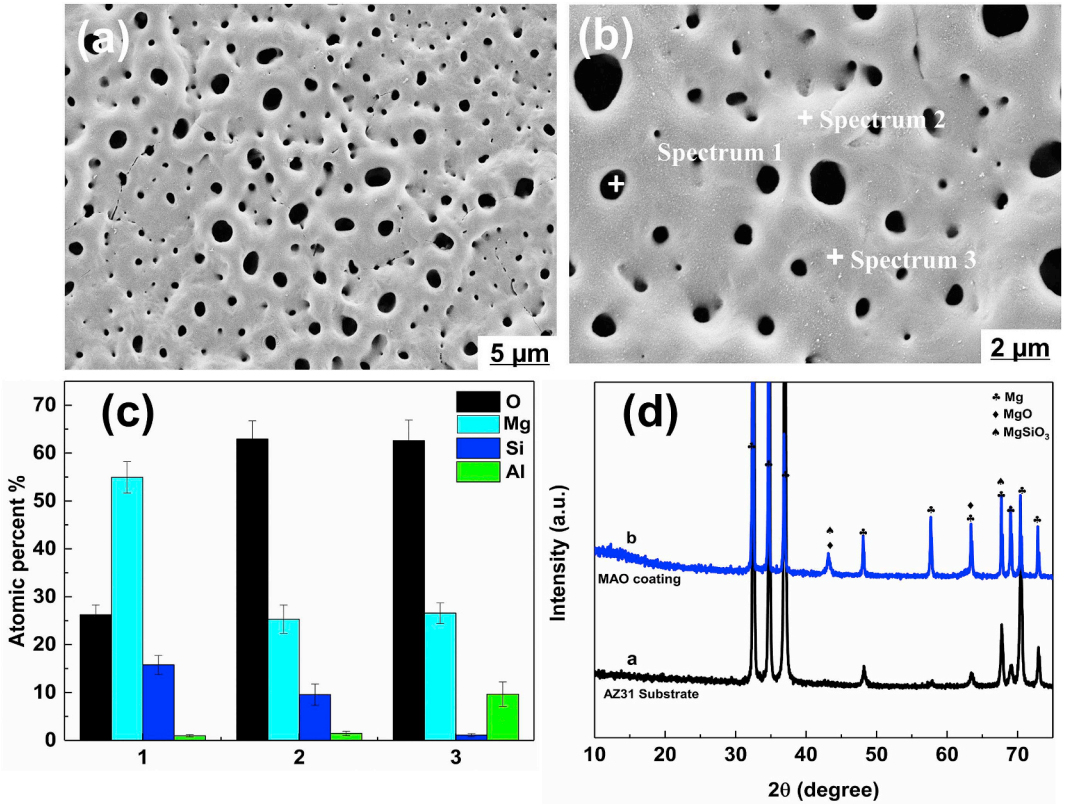

Fig. 2. SEM images (a, b) and elemental compositions (c) of MAO coating; XRD patterns (d) of AZ31 substrate and its MAO coating.

was recorded using Al Kα radiation (hv = 1486.6 eV) as excitation source.

2.4. Degradation characterization

2.4.1. Electrochemical tests

The open-circuit potential (OCP), potentiodynamic polarization curves (Tafel) and electrochemical impedance spectroscopy (EIS) were employed to investigate the corrosion resistance of the samples in phosphate buffer saline (PBS, pH 7.4; 8.0 g/L NaCl, 0.2 g/L KCl, 1.44 g/L Na_2HPO_4 and 0.24 g/L KH_2PO_4) with or without bovine serum albumin (BSA, 1 g/L). The BSA-containing solution was designated as BSA-PBS. The OCP, Tafel and EIS curves were recorded via an electrochemical analyzer (PAR Model 2273, Princeton, USA). A three-electrode cell consisting of a platinum counter electrode, a saturated calomel electrode (SCE), and samples as working electrode was used [4]. The electrochemical data (corrosion current density (i_{corr}) and corrosion potential (E_{corr})) were obtained through Tafel extrapolation method. The i_{corr} ($A{\cdot}cm^{-2}$) was converted to degradation rate, P_i ($mm{\cdot}year^{-1}$), using the following formula [37]:

$$P_i = 0.02285\ i_{corr} \quad (1)$$

To ensure reproducibility, all experiments were done in triplicate.

2.4.2. Immersion tests

The immersion tests were used to evaluate the degradation rate of AZ31 Mg substrate and its MAO coating. The samples were soaked in PBS and BSA-PBS solution at 310 K under an inverted funnel connected to a graduated acid burette (Fig. 7a), and the solution level was intermittently measured (1 h) for 150 h. The immersion tests were performed in quadruplicate. HER, V_H ($mL{\cdot}cm^{-2}\ h^{-1}$) can be expressed as:

$$V_H = V/st \quad (2)$$

where V is the hydrogen evolution volume (HEV), s and t are the exposed area of the samples and soaking time, respectively. The HER, V_H ($mL{\cdot}cm^{-2}\ h^{-1}$), can be represented as the degradation rate, P_H ($mm{\cdot}year^{-1}$), using the following relationship [38]:

$$P_H = 54.696 V_H \quad (3)$$

2.5. Cytotoxicity tests

Human osteosarcoma (MG63) cells were used for cytotoxicity tests. The cells were cultured in a standard culture medium containing Eagle's Minimum Essential Medium (EMEM, GIBCO) supplemented with 1% penicillin/streptomycin (ATCC) and 10% fetal calf serum (FCS, BOVOGEN) at 37 °C in a humidified atmosphere of 5% CO_2.

The MG63 cells (1×10^4 cells/mL,4 mL) were seeded on sterilized samples, and cultured for up to 72 h in 6-well tissue culture test plates. Subsequently, 400 μL MTT (5 mg/mL in PBS, MCE) were added into 6-well tissue culture test plates for 4 h at 37 °C in 5% CO_2 atmosphere. Then, the dimethyl sulfoxide was employed to sufficiently dissolved the crystals in each well by shaking it at a low speed for 10 min. The proliferation of MG63 cells on the sample was measured after 24 and 72 h by the absorbance of a microplate reader (Epoch2T, Biotek) at a wave length of 570 nm. The MG63 cells (cultured cells for 24 h) were fixed in 2.5% glutaraldehyde and dehydrated in a series of graded ethanol solutions (50, 75 and 100%) at room temperature. Then, the hexamethyldisilazane was applied to preserve the original morphology of the MG63 cells. SEM was employed to observe the morphology of MG63 cells on the samples. The Calcein (stain live cells) and PI (stain dead cells) were obtained from Thermo Fisher Scientific and stained the MG63 cells on the samples. Fluorescence microscope (FM) was used to observe the MG63 cells (cultured cells for 72 h) by excitation wavelength of 488 nm. All tests were performed in triplicate.

2.6. Statistical analysis

Statistical analysis was employed by the independent-samples *t*-test. Difference was considered significant at **P < 0.01 or *P < 0.05.

3. Results

3.1. Surface analysis

SEM images of the MAO coating are shown in Fig. 2, where the porous structure of the MAO coating was revealed (Fig. 2a and b). The elemental composition (Spectrums #1–3) of the coating was mainly Mg, O and Si as well as trace of Al (Fig. 2c), indicating the presence of $MgSiO_3$ and MgO, which was related to plasma chemical oxidation reactions between the Mg substrate and the electrolyte in the discharging channels produced by the sparks. During the process, SiO_3^{2-} and OH^- ions, etc. migrated inward into the channels under the electrical field, whereas the dissolving Mg^{2+} ions migrated outward from the substrate. And this result of SEM image is in pronounced agreement with the XRD patterns (Fig. 2d), where MAO coating exhibited characteristic peaks of $MgSiO_3$ and MgO, and Mg peaks were observed for uncoated AZ31 Mg substrate.

3.2. Electrochemical tests

The OCP curves of the samples in PBS and BSA-PBS solution were recorded (Fig. 3a). In the PBS solution, the OCP value of AZ31 Mg substrate fluctuated rapidly before 250 s of immersion, which can be interpreted as the formation of the degradation product ($Mg(OH)_2$) and subsequent dissolution due to the aggressive Cl^- ions [39,40]. Thereafter, the OCP slowly reached a relatively stable value owing to the balance in the formation and dissolution of $Mg(OH)_2$ [41]. A slow raise and gradually stabilization of OCP values (AZ31 substrate, BSA-PBS) was observed, which can be related to the absorption of BSA, inhibiting the dissolution of $Mg(OH)_2$. The OCP curve of MAO coating showed stable values, indicating that the MAO coating effectively suppressed the dissolution of the Mg alloy [37]. The OCP values of the MAO coating exhibited significant increase with increase in time due to the adsorption of BSA [42]. Compared with the final OCP values of the samples in PBS solution, the addition of protein shifted the OCP to a more positive value, suggesting that the adsorption of BSA significantly changed the electrochemical behavior [43].

Fig. 3b shows the polarization curves of the samples in PBS and BSA-PBS solution, the obtained i_{corr} values of the samples could be ranked in an increasing order as follows: 5.38×10^{-9} A cm^{-2} (MAO coating, BSA-PBS) < 4.36×10^{-8} A cm^{-2} (MAO coating, PBS) < 8.78×10^{-6} A cm^{-2} (AZ31 substrate, BSA-PBS) < 1.98×10^{-5} A cm^{-2} (AZ31 substrate, PBS), indicating that the MAO coating possessed a more effective corrosion protection (Table 1) [44,45]. There is a breakdown potential (E_1) in the anodic branch of the Tafel curve of the MAO coating (BSA-PBS), which could be attributed to the breakdown of BSA-MAO film. The electrochemical results indicated that the addition of BSA improve the corrosion resistance of the samples, which could be explained by the thermodynamics of Arrhenius equation [35]:

$$i_{corr} = A\, e^{\frac{-Ea}{RT}} \quad (4)$$

where i_{corr} is corrosion current density (A·cm^{-2}). *Ea* is corrosion activation energy (J·mol^{-1}), *A* refers a pre-exponential factor. *T* and *R* are the absolute temperature and gas constant, respectively. According to Eq. (4), the adsorption of BSA on samples could effectively enhance *Ea* required for degradation and improve the electrochemical stability, which could inhibit the degradation behavior [46,47]. The obtained result is consistent with the literature reports [48].

Nyquist plots of the samples are presented in Fig. 4a. The AZ31 Mg substrate displayed a small inductive loop and two capacitance loops in the PBS and BSA-PBS solution, which can be attributed to pitting corrosion and charge transfer reaction, respectively [49,50]. For MAO coating, an inductive loop in the low frequency range and a capacitance loop in the medium frequency ranges could be observed in the PBS solution, suggesting that the pitting corrosion due to flaking of the coating and the charge transfer process, respectively [51]. Moreover, the larger capacitance loop suggested better corrosion resistance. The corrosion resistance of the samples could be ranked in an increasing order as follows: AZ31 Mg substrate (PBS) < AZ31 Mg substrate (BSA-PBS) < MAO coating (PBS) < MAO coating (BSA-PBS), confirming that the BSA protected the AZ31 Mg substrate and its MAO coating from corrosion. The result was because the adsorbed BSA changed the electric field and reduced the conductivity of the surface [48].

Typically, a high modulus |Z| value suggests that the sample has better corrosion resistance [1]. In this study, the |Z| of samples at the low-frequency were: 1.33×10^3 Ω cm^2 (AZ31 substrate, PBS), 2.53×10^3 Ω cm^2 (AZ31 substrate, BSA-PBS), and 102.65×10^3 Ω cm^2 (MAO coating, PBS) together with 326.90×10^3 Ω cm^2 (MAO coating, BSA-PBS), respectively (Fig. 4b). This consequence confirmed that BSA improved the corrosion resistance of the samples.

Fig. 4c shows the equivalent circuit ($R_s(Q_1(R_{ct}(Q_2(LR_L))))$) used to fit the EIS plots of AZ31 Mg substrate. In the circuit model, the solution resistance is represented by R_s. *Q* is the constant phase element (*CPE*), which denotes a pure capacitance for the coating capacitance and the

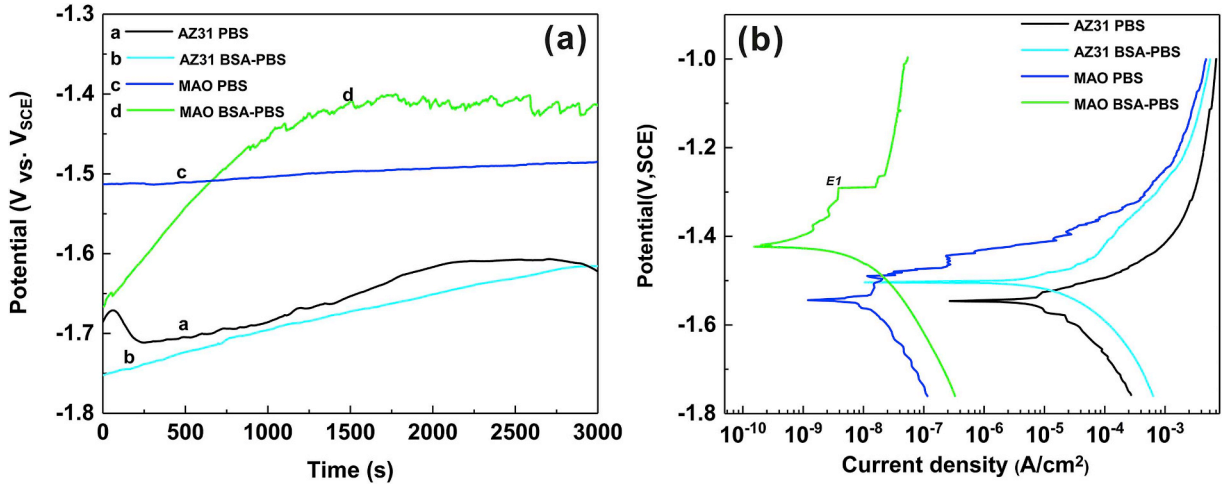

Fig. 3. OCP curves (a) and potentiodynamic polarization curves (b) of AZ31 substrate and its MAO coating in PBS and BSA-PBS solution.

Table 1
Electrochemical parameter of the AZ31 Mg substrate and its MAO coating.

Samples	AZ31 (PBS)	AZ31 (BSA-PBS)	MAO (PBS)	MAO (BSA-PBS)
E_{corr} (V, SCE)	−1.56	−1.51	−1.53	−1.42
i_{corr} (A·cm^{-2})	1.98 × 10^{-5}	8.78 × 10^{-6}	4.36 × 10^{-8}	5.38 × 10^{-9}
P_i (mm·year^{-1})	4.52 × 10^{-1}	2.00 × 10^{-1}	9.94 × 10^{-4}	1.20 × 10^{-4}

double layer capacitance between the coating and the metal substrate [37]. R_{ct} represents charge transfer resistance. The inductive loop is represented by R_L and L in series, which indicates the presence of pitting corrosion at the low frequency. For MAO coatings in PBS solution, the following equivalent circuit is used: $R_s(Q_1(R_{f1}(Q_2R_{ct})))$ (Fig. 4d), where R_{f1} is coating resistance. In the case of MAO coating in BSA-PBS solution, following equivalent circuit is usedd: $R_s(C_1(R_1(Q_1(R_{f1}(Q_2R_{ct}))))$ (Fig. 4e), C_1 represents the adsorbed protein layer capacity [52]. The R_{ct} of samples could be ranked in an increasing order as follows: AZ31 substrate (PBS, 9.06 × 10^2 Ω cm^2) < AZ31 substrate (BSA-PBS, 1.78 × 10^3 Ω cm^2) < MAO coating (PBS, 1.28 × 10^5 Ω cm^2) < MAO coating (BSA-PBS, 4.16 × 10^5 Ω cm^2) (Table 2). This finding is consistent with the results from potentiodynamic polarization curves.

3.3. Immersion tests

The XPS spectra were used to determine the surface composition of AZ31 Mg substrate and its MAO coating after soaked in BSA-PBS solution for 10 s, as shown in Fig. 5. The O 1s, N 1s, C 1s and P 2p together with Mg 2p could be observed in the XPS survey spectra (Fig. 5a). In C 1s spectra (Fig. 5b–1 and b-2), three peaks at 284.5, 285.6 and 287.7 eV, which were assigned to C–C/C–H, C–O/C–N and N–C═O, respectively [52]. The N 1s of AZ31 substrate (Fig. 5c–1) and MAO coating (Fig. 5c–2) demonstrated two peaks with binding energies associated with N–C/N–O (399.4 eV) and O═C–NH-(C, H) (400.08 eV) [53]. These results indicated the presence of BSA on the AZ31 Mg substrate and its MAO coating. Moreover, the Mg 2p spectra of AZ31 substrate could be split into two peaks: MgO (50.3 eV) and $Mg(OH)_2$ (49.6 eV), corresponding to corrosion products (Fig. 5d–1). The BSA molecules probably reacted with Mg^{2+} ions ($Mg(OH)_2$) to form $(RCH(NH_2)COO)_2Mg$ and absorbed on the AZ31 substrate (Reaction 5), which was in good agreement with previous study of our group [32].

$$Mg(OH)_2 + 2RCH(NH_2)COOH \rightarrow (RCH(NH_2)COO)_2Mg + 2H_2O \quad (5)$$

Whereas the Mg 2p spectra of MAO coating (Fig. 5d–2) only showed a MgO peak (50.3 eV), indicating that the MAO coating did not occur the corrosion behavior after immersed in BSA-PBS solution for 10 s, which was because the absorbed BSA on the MAO surface prevented the penetration of corrosive medium.

After 1 h of immersion in PBS solution, the AZ31 substrate showed severe corrosion morphology (Fig. 6a–1). The elements of corrosion products were mainly composed of Mg and O (Fig. 6a–2), suggesting $Mg(OH)_2$. The degradation degree of Mg substrate was decreased with the addition of BSA in the PBS solution, as shown in Fig. 6b–1. EDS spectra showed a trace of N (0.76 wt%; 1.05 at.%) on the AZ31 Mg substrate (Fig. 6b–2), which could be attributed to the existence of BSA on the surface; however, the BSA could not observed in the SEM images. The results might be attributed to the formation of $(RCH(NH_2)COO)_2Mg$. Differently, the MAO coating was still intact after 1 h immersion in the PBS and BSA-PBS solution. The results indicated that MAO coated substrate enhanced the corrosion resistance of the AZ31 Mg alloy (Fig. 6c–1 and d-1). When the MAO coating was soaked in the

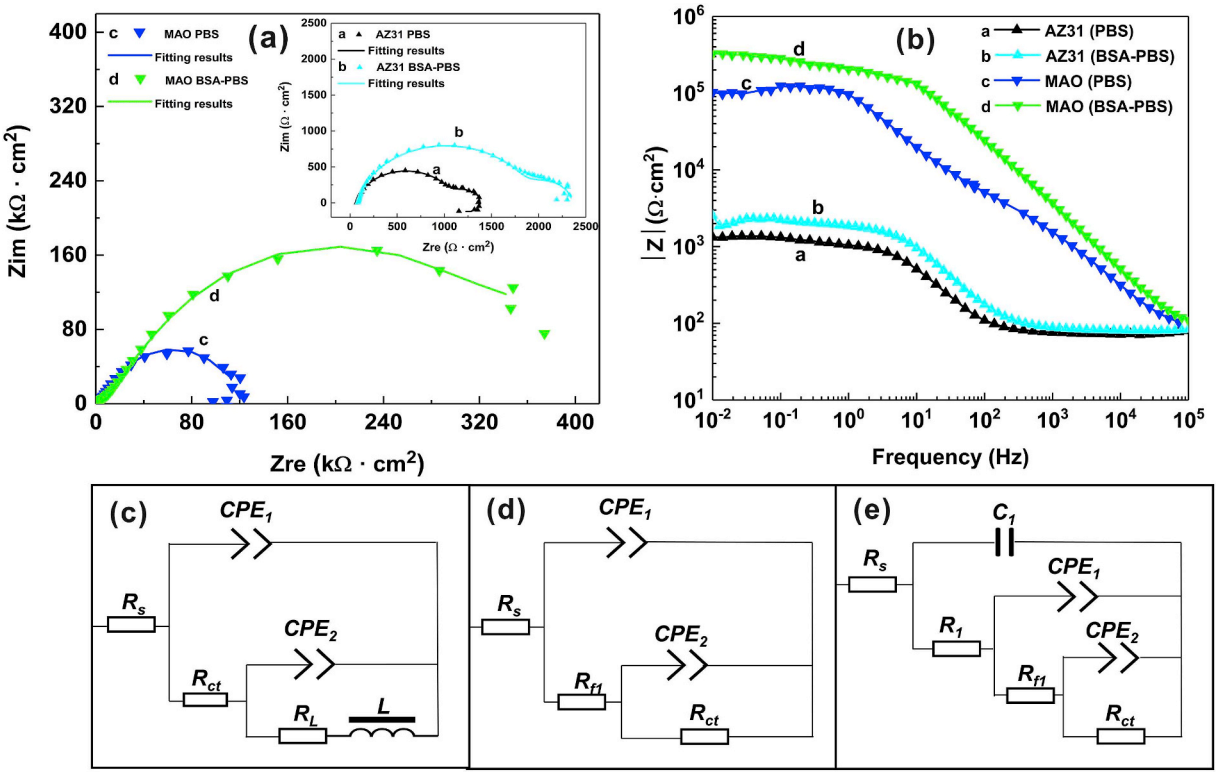

Fig. 4. EIS and the fitting results: (a) Nyquist plots and (b) Bode plots of AZ31 substrate and MAO coating; equivalent circuits of (c) AZ31 substrate in PBS and BSA-PBS solution, (d) MAO coating in PBS solution and (e) MAO coating in BSA-PBS solution.

Table 2
Electrochemical data obtained from equivalent circuit fitting of EIS curves.

Samples	R_s ($\Omega \cdot cm^2$)	C	R_1 ($\Omega \cdot cm^2$)	CPE_1 ($\Omega^{-1} \cdot cm^{-2} \cdot S^n$)	n_1	R_{f1} ($\Omega \cdot cm^2$)	CPE_2 ($\Omega^{-1} \cdot cm^{-2} \cdot S^n$)	n_2	R_{ct} ($\Omega \cdot cm^2$)	R_L ($\Omega \cdot cm^2$)	L ($H \cdot cm^{-2}$)
AZ31 (PBS)	73.82	–	–	3.88×10^{-5}	0.92	–	3.60×10^{-3}	0.30	9.06×10^{2}	235	3806
AZ31 (BSA-PBS)	81.82	–	–	2.13×10^{-5}	0.90	–	3.39×10^{-3}	0.39	1.78×10^{3}	170	2697
MAO (PBS)	64.12	–	–	5.84×10^{-7}	0.78	6172	6.03×10^{-7}	0.88	1.28×10^{5}	–	–
MAO (BSA-PBS)	66.81	1.09×10^{-8}	2566	2.31×10^{-7}	0.76	1685	3.31×10^{-7}	0.80	4.16×10^{5}	–	–

Table 3
Corrosion rates of the AZ31 Mg substrate and MAO coating after different immersion period, $mm \cdot year^{-1}$.

Samples	1 h	50 h	150 h
AZ31 substrate (PBS)	2.10	0.42	0.27
AZ31 substrate (BSA-PBS)	2.05	0.36	0.15
MAO coating (PBS)	0.00	0.16	0.08
MAO coating (BSA-PBS)	0.00	0.05	0.03

BSA-PBS solution for 1 h, the appearance of N (5.14 wt%; 6.68 at.%) revealed that the BSA was absorbed on the surface of MAO coating (Fig. 6d–2). And it could be clearly observed that the adsorbed BSA sealed the pores of the MAO coating, thereby further enhanced the corrosion resistance by forming a barrier layer.

Hydrogen evolution tests were used to investigate the degradation rate of the samples [54]. Fig. 7b shows the hydrogen evolution volume (HEV) of the samples. The HEV of the samples is ranked in decreasing order as follows: AZ31 Mg substrate (PBS, 0.48 ± 0.079 mL cm^{-2}) > AZ31 Mg substrate (BSA-PBS, 0.42 ± 0.087 mL cm^{-2}) > MAO coating (PBS,

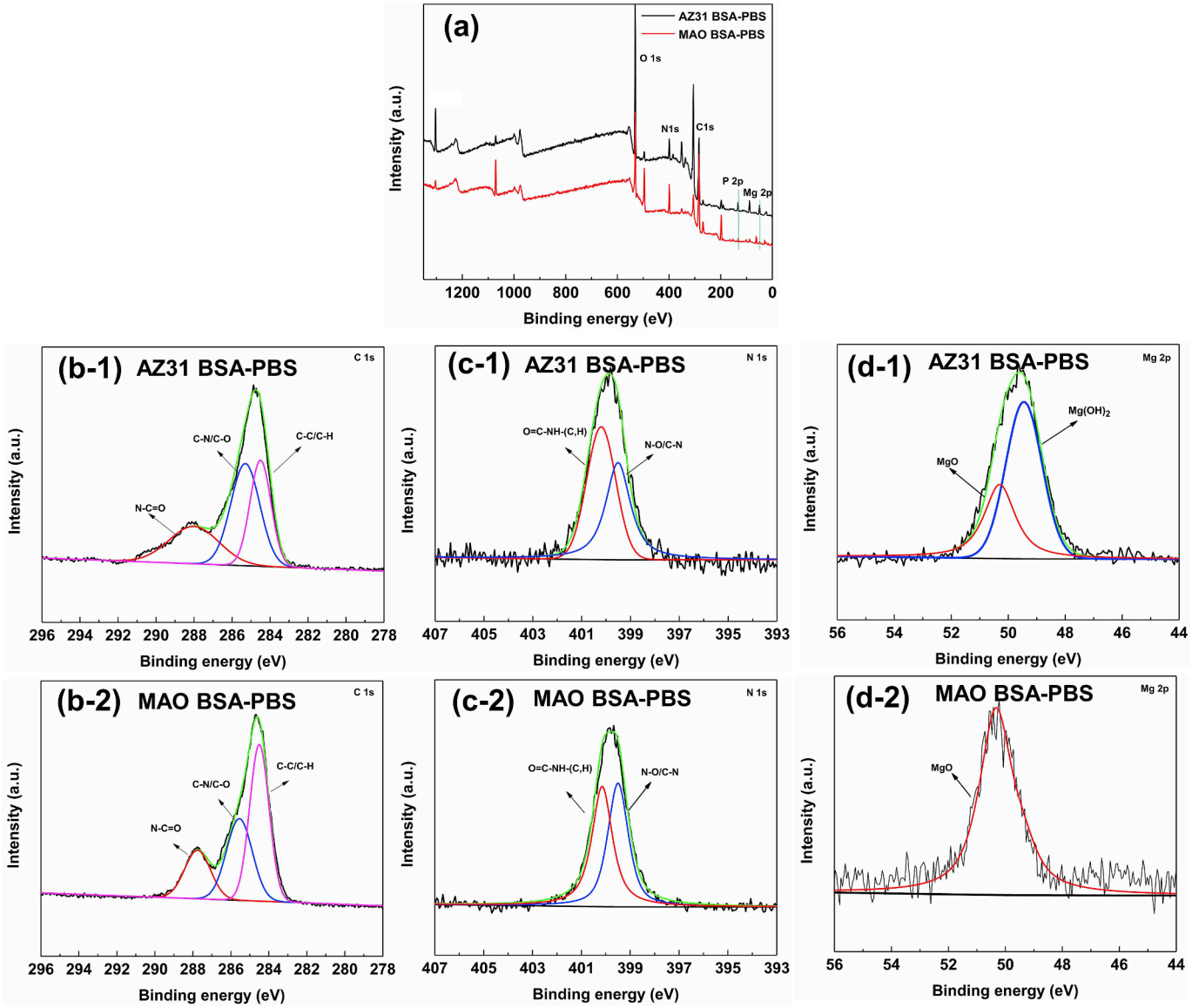

Fig. 5. XPS spectra of AZ31 substrate and its MAO coating after immersion in BSA-PBS solution for 10 s: (a) XPS survey, (b-1, b-2) C 1s, (c-1, c-2) N1s and (d-1, d-2) Mg 2p.

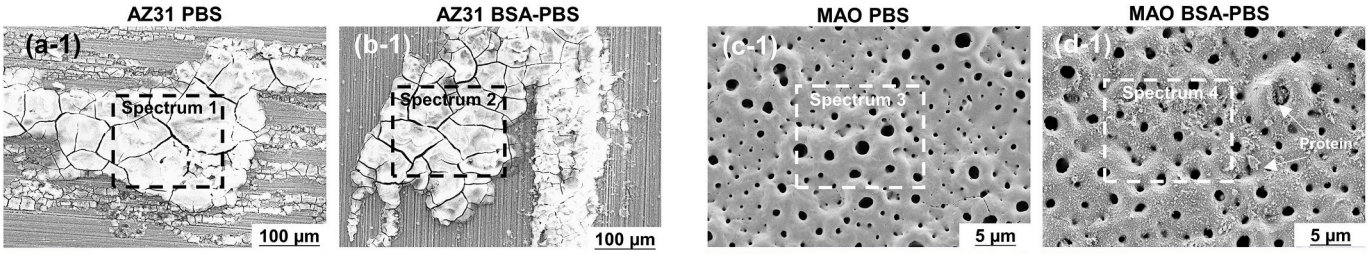

(a-2)	Weight (%)	Atom (%)
C	0.57	0.94
N	0.00	0.00
O	40.29	50.39
Mg	59.14	48.67

(b-2)	Weight (%)	Atom (%)
C	0.68	1.11
N	0.76	1.05
O	45.43	55.29
Mg	53.13	42.55

(c-2)	Weight (%)	Atom (%)
C	0.37	0.60
N	0.00	0.00
O	49.99	60.04
Mg	49.72	39.37

(d-2)	Weight (%)	Atom (%)
C	4.63	7.02
N	5.14	6.68
O	48.34	54.96
Mg	41.89	31.34

Fig. 6. SEM images of (a-1, b-1) AZ31 substrate and (c-1, d-1) MAO coating and corresponding EDS of (a-2, b-2) AZ31 substrate and (c-2, d-2) MAO coating after an immersion of 1 h in PBS and BSA-PBS solution.

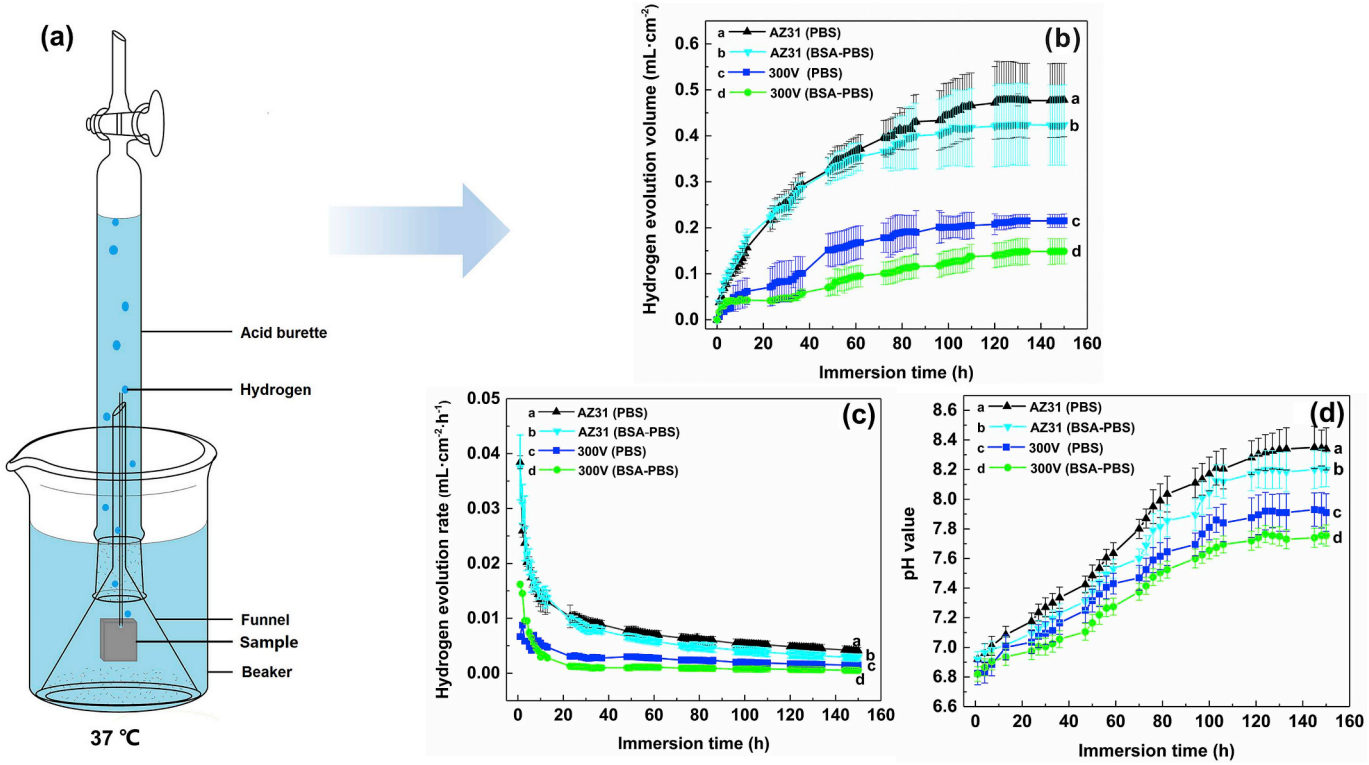

Fig. 7. (a) Schematic diagram of immersion tests; (b) Hydrogen evolution volume (HEV), (c) Hydrogen evolution rate (HER) and (d) pH value as a function of immersion time for AZ31 substrate and its MAO coating in PBS and BSA-PBS solution for 150 h.

0.22 ± 0.015 mL cm^{-2}) > MAO coating (BSA-PBS, 0.15 ± 0.028 mL cm^{-2}). The results suggested that adsorption of BSA improved the corrosion resistance of the samples [52]. Fig. 7c shows the hydrogen evolution rate (HER) of samples. The HER for specimen is ranked in increasing order as follows: MAO coating (BSA-PBS, (0.99 ± 0.45) × 10^{-3} mL $cm^{-2} \cdot h^{-1}$) < MAO coating (PBS, (1.44 ± 0.58) × 10^{-3} mL $cm^{-2} \cdot h^{-1}$) < AZ31 substrate (BSA-PBS, (2.83 ± 0.59) × 10^{-3} mL $cm^{-2} \cdot h^{-1}$) < AZ31 substrate (PBS, (3.19 ± 1.19) × 10^{-3} mL $cm^{-2} \cdot h^{-1}$). The change in pH of samples was also recorded in the immersion stage (Fig. 7d). The pH of MAO coating exhibited the smallest values in BSA-PBS solution after 150 h of immersion, suggesting that MAO coating possessed a slowest degradation rate, which could be related to the adsorption of BSA on the MAO coating.

Fig. 8 shows the typical surface morphologies of the samples after immersion in PBS and BSA-PBS solution for 150 h. The AZ31 Mg substrate suffered severe corrosion and large cracks in PBS solution (Fig. 8a–1 and a-2). The presence of O, Mg and P in the corrosion product suggests that they correspond to $Mg(OH)_2$ and insoluble phosphate compound (Table 4). In BSA-PBS solution, the degradation morphology of AZ31 Mg substrate was not significant (Fig. 8b–1 and b-2). The surface elements contained O, Mg, N and P (Table 4), suggesting the presence of $Mg(OH)_2$, $(RCH(NH_2)COO)_2Mg$ and phosphates [32]. Interestingly, an increase in the N/P ratio was observed (Table 4), which could be interpreted as the competitive adsorption of BSA and phosphates [52]. When MAO coating was immersed in BSA-PBS solution (Fig. 8d–1 and d-2), the corrosion pits was not evident and remained relatively less attacked as compared to that in PBS solution (Fig. 8c–1 and c-2).

In order to analyze the degradation products of the samples, XRD and FT-IR analysis were done. From the XRD patterns (Fig. 9a), it was

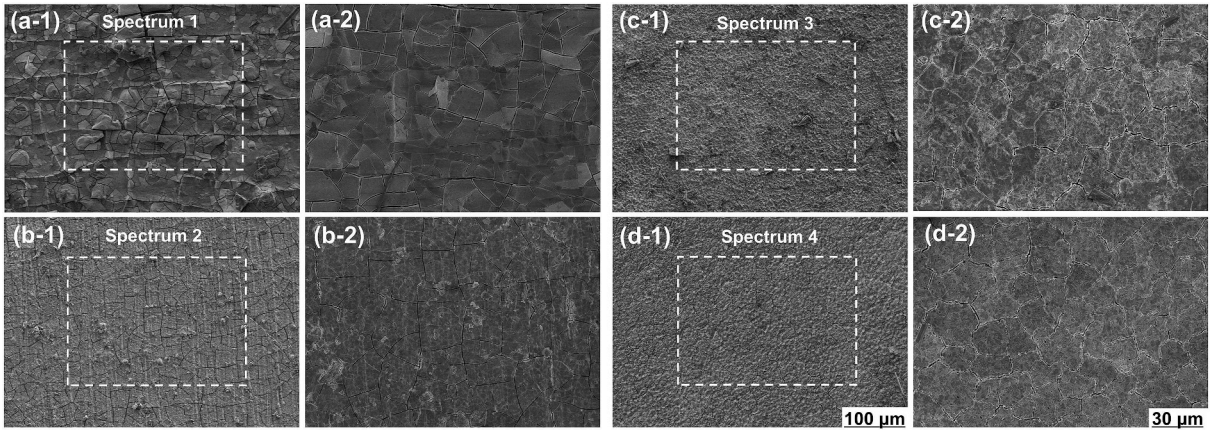

Fig. 8. SEM morphologies and elements analysis of AZ31 substrate (a, b) and MAO coating (c, d) after 150 h of immersion in (a, c) PBS solution and (b, d) BSA-PBS solution.

Table 4
Elemental compositions (in wt/at. %) of samples immersed in PBS and BSA-PBS solution.

Samples	C	O	Mg	N	P	N/P
AZ31 PBS (#1)	19.64 (29.31)	33.65 (43.08)	13.92 (10.27)	0.39 (0.55)	23.11(14.53)	0.017 (0.038)
AZ31 PBS-BSA (#2)	13.42 (20.18)	45.47 (51.32)	15.43 (12.49)	4.60 (6.36)	11.59 (7.34)	0.397 (0.870)
MAO PBS (#3)	17.93 (27.01)	40.44 (45.74)	14.14 (10.52)	0.23 (0.46)	16.42 (9.59)	0.014 (0.048)
MAO BSA-PBS (#4)	10.69 (16.08)	48.22 (56.01)	12.33 (9.66)	4.66 (5.89)	6.84 (3.99)	0.681 (1.470)

found that the main degradation products were $Mg(OH)_2$ for AZ31 Mg substrate in PBS solution. Small quantities of insoluble phosphates (i.e. $Mg_3(PO_4)_2$) were also observed. However, when AZ31 Mg substrate was immersed in the BSA-PBS solution, the peak of $Mg(OH)_2$ was not evident. For MAO coating, the peak intensity of $Mg(OH)_2$ in PBS solution was higher than that in BSA-PBS solution. In the FT-IR spectra of the samples (Fig. 9b), the absorption peak at 3420 cm^{-1} was attributed to –OH, which was from the degradation product ($Mg(OH)_2$). The bands at approximately 1650 cm^{-1}, 1051 cm^{-1} and 565 cm^{-1} corresponded to PO_4^{3-} ions, indicating the presence of $Mg_3(PO_4)_2$, which agreed with the results of XRD pattern (Fig. 9a).

3.4. Cells response tests

Fig. 10a shows the cell number count after 24 and 72 h cells response test. MG63 cell number continuously increased during the incubation period, especially in the first 24 h. For AZ31 Mg substrate, the number of cells decreased (cultured cell in 72 h) because of rapid degradation and increase in the localized pH value, which inhibited the cells proliferation [55]. However, the cell number of MAO coating was slightly higher. Results suggested that MG63 cells preferred the surfaces with relatively high amplitude of micro-roughness. A significant increase in MG63 cells density was observed after 72 h of incubation as compared with the seeding cells density. The results indicated that MAO coating displayed good viability with MG63 cells and thus possessed desirable bioactivity because the MAO coatings mainly composed of MgO [26]. The MG63 cells attachment morphology is shown in Fig. 10b. For AZ31 Mg substrate, MG63 cells (cultured cell in 24 h) exhibited a thin and flat shape on the surface (Figs. 10b–1). Interestingly, unlike AZ31 Mg substrate, MG63 cells (cultured cell in 24 h) were rounded shaped and attached tightly on sample surface by spreading with extension of filopodia into micropores on MAO surface (Fig. 10b–2) [56].

To further investigate the MG63 cells proliferation and morphology on the samples, live/dead staining of cells after cultured 72 h was done and shown in in Fig. 10c (live cell-green, dead cell-orange-red). MG63

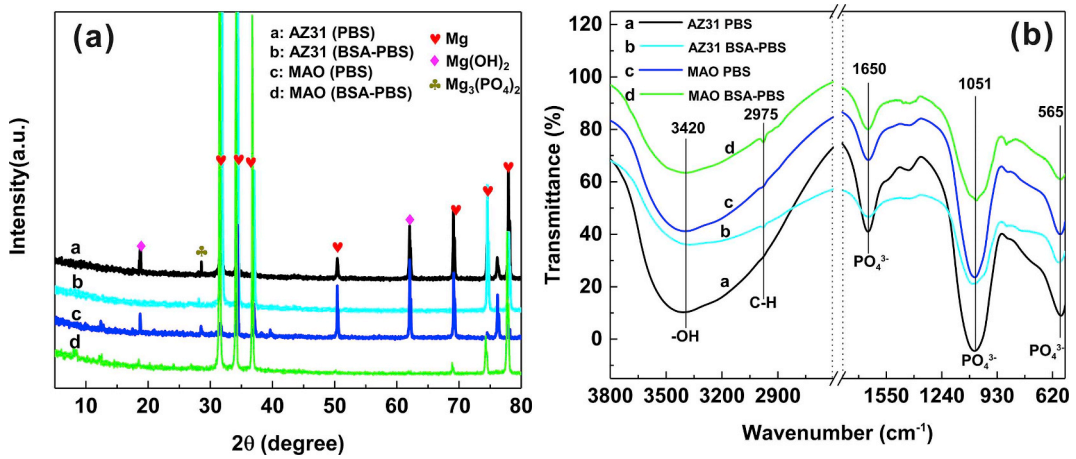

Fig. 9. XRD patterns (a) and FT-IR spectra (b) of AZ31 substrate and its MAO coating in PBS and BSA-PBS solution after 150 h of immersion.

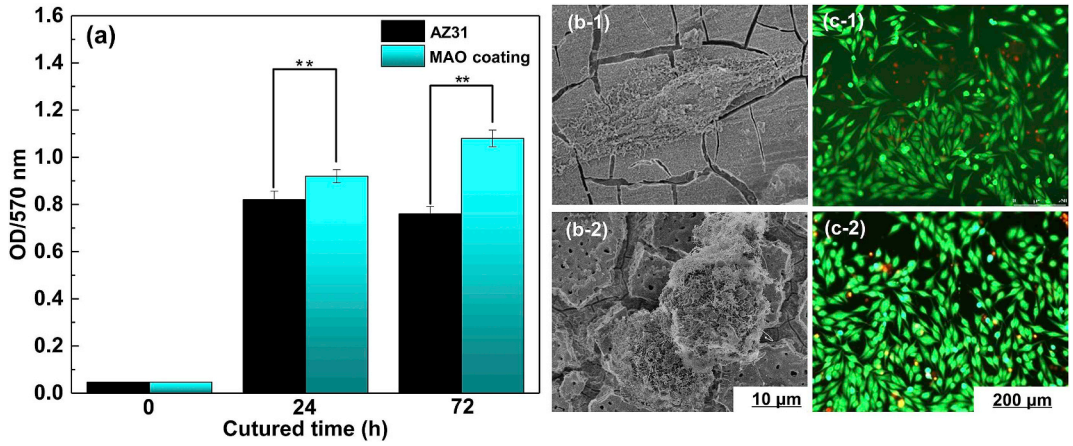

Fig. 10. MG 63 cells response to (a) the AZ31 substrate and MAO coating of cell proliferation after 24 and 72 h incubation; Statistically significant differences (*P < 0.05, **P < 0.01); SEM morphology of MG63 cells to (b-1) AZ31 substrate and (b-2) MAO coating after 24 h incubation; Live/Dead of MG63 cells after 72 h incubation: (c-1) AZ31 substrate and (c-2) MAO coating.

cells exhibited healthy fusiform-like shape, and were randomly distributed on the samples. Only a small number of dead cells were observed, suggesting that AZ31 Mg substrate and its MAO coatings possessed an acceptable cytocompatibility to MG63 cells [57].

4. Discussion

The degradation rates P_i (Table 1) and P_H (Table 3) values obtained from different approaches (Tafel extrapolation and hydrogen evolution rate) showed a similar trend. The i_{corr} was determined through the cathodic slope [58], whereas, P_H was calculated by the HER of Mg alloys, which was similar to the weight loss rate [59,60].

4.1. Comparison of the effects of protein on samples

Table 5 shows a comparison of literature data on the effects of protein on pure Mg, Mg alloys and their coating. Mueller et al. [61] found that protein could increase the degradation rates of pure Mg in PBS solution; the lower the concentration, the higher the degradation rate. The degradation product layer was not uniform and did not offer protection to the entire surface. Heakal et al. [62] showed that the addition of 10–20 g/L BSA retarded Mg alloy AZ80 degradation through a complete adsorbed layer. However, at lower concentration of BSA < 10 g/L, it accelerated the dissolution of Mg alloy via metal chelation; and at higher concentration of BSA > 20 g/L, it stimulated the degradation of Mg alloy because of protein aggregation. Interestingly, Wang et al. [35] reported that the quick adsorption of albumin effectively protected the Mg alloy at initial stage, and a chelation effect accelerated the degradation rate of Mg alloy with increasing soak time. However, in this study, the addition of BSA inhibited the degradation behavior of Mg alloys AZ31 because BSA ($RCH(NH_2)COO^-$) combined with Mg^{2+} to form $(RCH(NH_2)COO)_2Mg$ and thereby prevented the absorption of Cl^- ions [32]. For the MAO-coated sample, Wan et al. [52] reported that the addition of albumin hindered the dissolution of the Mg/PEO coating. In this case, protein was adsorbed on the surface and thus provided protection at the early stage of immersion. Then, the gradual formation of $(RCH(NH_2)COO)_2Mg$ further protected the samples from attack with immersion time. The biodegradation mechanism of the samples in the PBS and BSA-PBS solution was discussed in Section 4.3.

4.2. Degradation mechanism

4.2.1. Influence of protein on degradation of AZ31 substrate

The degradation behavior of AZ31 substrate in PBS and BSA-PBS solution were investigated (Fig. 11). When immersed in PBS solution (Fig. 11a–c), immediately, a thin layer of $Mg(OH)_2$ was formed on the surface of AZ31 Mg substrate (Fig. 11a). The reactions are as follows [63]:

Anodic reaction:

Table 5
Influence of protein on pure Mg, Mg alloys and its coating (↑: acceleration; ↓: inhibition).

Material	Solution	i_{corr} (A/cm^2)	E_{corr} (V/SCE)	Effects	Refs
Pure Mg	PBS	$(7.76 \pm 8.81) \times 10^{-6}$	-1.18 ± 0.09		[61]
	PBS + 0.1 g/L albumin	$(3.53 \pm 3.39) \times 10^{-4}$	-1.42 ± 0.03	↑	
	PBS + 1 g/L albumin	$(1.26 \pm 7.56) \times 10^{-5}$	-1.43 ± 0.04	↑	
	PBS + 10 g/L albumin	$(3.73 \pm 5.41) \times 10^{-5}$	-1.34 ± 0.06	↑	
AZ80	SBP	2.82×10^{-6}	-1.44		[62]
	SBP + 5 g/L BSA	3.98×10^{-6}	-1.45	↑	
	SBP + 10 g/L BSA	1.01×10^{-6}	-1.42	↓	
	SBP + 20 g/L BSA	1.78×10^{-6}	-1.42	↓	
	SBP + 40 g/L BSA	3.37×10^{-6}	-1.45	↑	
M1A	SBF	3.62×10^{-4}	-1.82		[35]
	SBF + 40 g/L albumin	2.81×10^{-4}	-1.71	First ↓ Then ↑	
AZ31	PBS	1.98×10^{-5}	-1.56		Present work
	PBS + 1 g/L BSA	8.87×10^{-6}	-1.51	↓	
Pure Mg/PEO	PBS	1.63×10^{-8}	-1.69		[52]
	PBS + 1 g/L albumin	2.56×10^{-9}	-1.71	↓	
AZ31/MAO	PBS	4.36×10^{-8}	-1.53		Present work
	PBS + 1 g/L BSA	5.38×10^{-9}	-1.42	↓	

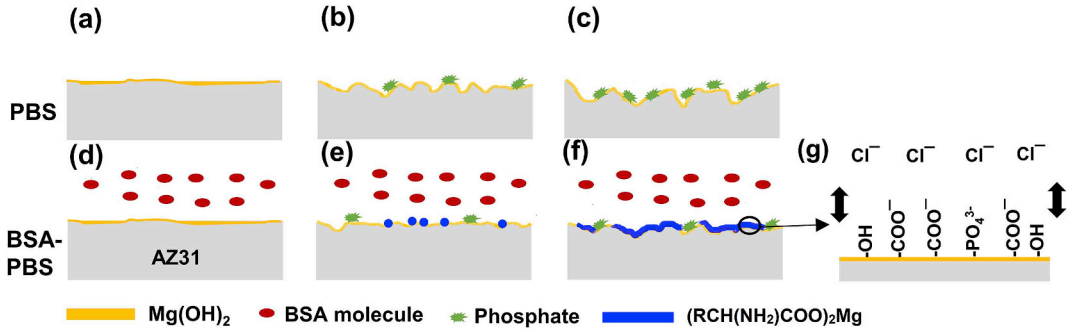

Fig. 11. Degradation mechanism of AZ31 substrate: (a–c) in PBS solution and (d–g) in BSA-PBS solution.

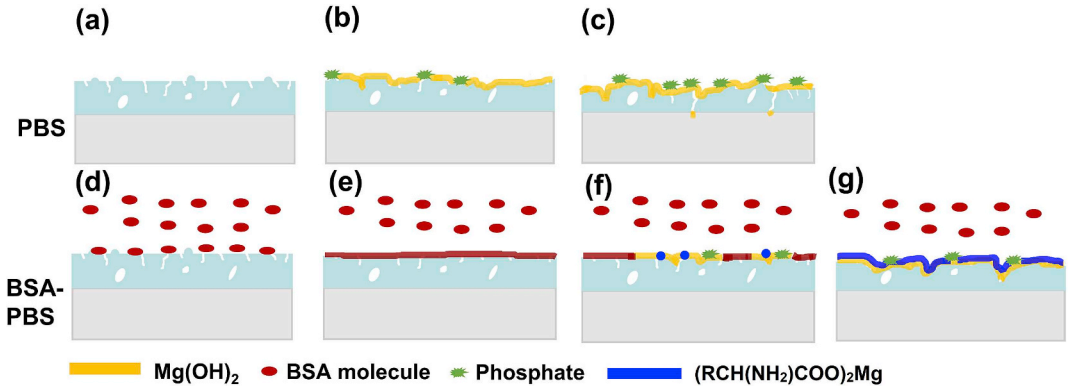

Fig. 12. Degradation mechanism of MAO coatings: (a–c) in the PBS solution and (d–g) in BSA-PBS solution.

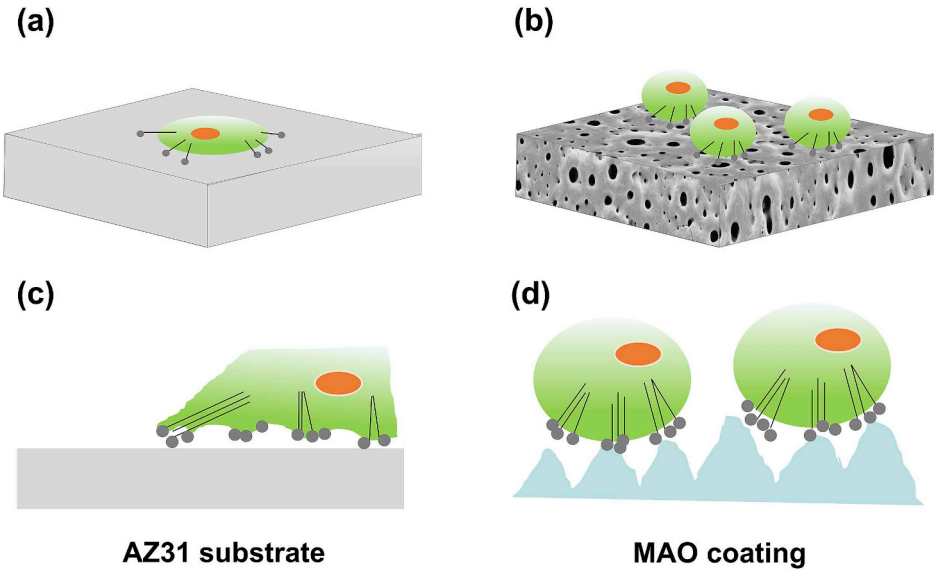

Fig. 13. Schematic illustration of the cell proliferation and morphology of (a) and (c) AZ31 substrate, (b) and (d) MAO coating.

$$Mg \rightarrow Mg^{2+} + 2\,e^{-} \quad (6)$$

Cathodic reaction:

$$2H_2O + 2\,e^{-} \rightarrow 2\,OH^{-} + H_2\uparrow \quad (7)$$

Total reaction:

$$Mg + 2H_2O \rightarrow Mg(OH)_2\downarrow + H_2\uparrow \quad (8)$$

With an increase in soaking time, more corrosion products were covered on AZ31 Mg substrate (Fig. 11b and c). Although $Mg(OH)_2$ film had protective properties, the aggressive Cl^- ions could dissolve the Mg $(OH)_2$ film by following reaction [39].

$$2Cl^{-} + Mg(OH)_2 \rightarrow MgCl_2 + 2OH^{-} \quad (9)$$

As the reaction proceeded, the formation and dissolution of degradation products reached chemical equilibrium, and the degradation rate gradually decreased. It has also been reported that phosphate (PO_4^{3-}) combines with Mg^{2+} ions to form $Mg_3(PO_4)_2$ on the surface (Reaction 12).

$$H_2PO_4^{-} \rightarrow HPO_4^{2-} + H^{+} \quad (10)$$

$$HPO_4^{2-} \rightarrow PO_4^{3-} + H^{+} \quad (11)$$

$$2PO_4^{3-} + 3Mg^{2+} \rightarrow Mg_3(PO_4)_2\downarrow \quad (12)$$

Interestingly, the degradation performance of AZ31 Mg substrate was significantly affected in the BSA-PBS solution. On the one hand, the $RCH(NH_2)COO^-$ group of BSA molecules, combined with Mg^{2+} ions and formed $(RCH(NH_2)COO)_2Mg$ on the surface of the AZ31 Mg substrate and prevented further degradation (Reaction 5) [32].

The plausible reason for only a trace of insoluble phosphates observed on the Mg surface could be due to the corrosion inhibiting effect of BSA (Fig. 11d–f) [52]. On the other hand, the negatively charged ions such as COO^-, PO_4^{3-} and OH^- prevented the attack of Cl^- ions from the solution by electrostatic repulsive effects (Fig. 11g). Hence, the synergistic protective effect from $(RCH(NH_2)COO)_2Mg$, $Mg(OH)_2$ and phosphates led to a reduced degradation rate [33].

4.2.2. Influence of protein on degradation of MAO coating

The degradation mechanism of MAO coating is shown in Fig. 12. When MAO coating was immersed in the PBS solution (Fig. 12a–c), the MAO coating acted as a physical barrier to protect the AZ31 Mg substrate. The chemical reaction of MgO with H_2O occurred as follows:

$$MgO + H_2O \rightarrow Mg(OH)_2\downarrow \quad (13)$$

With the increase of soaking time, Cl^- ions dissolved the degradation products ($Mg(OH)_2$) and the electrolyte slowly penetrated into the inner MAO layer owing to the micropores on the surface of MAO sample. Then, the electrochemical corrosion (Reaction 6–8) occurred on the samples. In addition, some insoluble phosphate formed on the surface by the reaction of PO_4^{3-} with Mg^{2+} ions.

The degradation behavior of MAO coatings was significantly influenced with the addition of BSA. In the PBS solution (pH 7.4), BSA showed negative charge (pI_{BSA}4.7 < pH 7.4) [32], whereas MAO coating possessed positive charge (pI_{MAO}12.4 > pH 7.4) [64]. A thin layer of BSA could be immediately absorbed on the surface due to the electrostatic attraction after immersed in BSA-PBS solution (Fig. 12d and e), and the absorbed dense BSA layer suppressed the degradation behavior to some degree by covering MAO surface or sealing the micro-pores.

After certain time, the degradation products ($Mg(OH)_2$) gradually formed on the MAO surface due to electrolyte permeation through the BSA layer. The BSA and PO_4^{3-} reacted with $Mg(OH)_2$ to form $(RCH(NH_2)COO)_2Mg$ and phosphates (Fig. 12f), respectively. Finally, the outer layer $(RCH(NH_2)COO)_2Mg$ and inner layer MAO coating were formed and synergistically protected the substrate (Fig. 12g).

4.3. Cell compatibility of samples

For AZ31 Mg substrate, the smooth surface inhibited the attachment of cell and thus decreased the cell proliferation (Fig. 13a) [65]. By contrast, MAO coating possessed high surface roughness, which provided a wider area for cell attachment and proliferation (Fig. 13b) [66]. In terms of cell morphology, the MG63 cells on the smooth surface of AZ31 substrate had a very intimate contact with the substrate through abundant filopodia, and dispersed randomly in all directions, exhibiting disordered orientations (Fig. 13c). Anselme's hypothesis could explain the phenomenon because the cell tended to find a favorable state to balance the internal and external forces [67]. For MAO coating (Fig. 13d), the rough surface exerted stronger constraints on the cell morphology, hence, the cell shape was round [26].

5. Conclusions

The interaction mechanism of proteins and MAO coatings on biodegradable Mg alloys was investigated. The following conclusions can be drawn from this study:

(1) The presence of protein in the electrolyte led to the formation of $(RCH(NH_2)COO)_2Mg$ since $RCH(NH_2)COO^-$ group of BSA molecules combined with Mg^{2+} ions of generated $Mg(OH)_2$, thus decreasing the degradation rates (P_i = 0.20 mm year^{-1};P_H = 0.15 mm year^{-1}) of Mg alloy AZ31 by preventing the attack of Cl^- ions.

(2) The adsorption of BSA on the MAO surface was caused by electrostatic attraction due to their different *pI*s (pI_{BSA}4.7 < pH 7.4; pI_{MAO}12.4 > pH 7.4), thereby serving as a protection layer at the early-immersion stage; and later the formation of $(RCH(NH_2)COO)_2Mg$ led to a fairly degradation rates (P_i = 0.00012 mm year^{-1}; P_H = 0.03 mm year^{-1}). Further, the electrochemical polarization results showed that the BSA addition shifted the OCP value toward a noble direction and resulted in a smaller corrosion current density.

(3) MG63 cells exhibited flattened and round shape on the Mg alloy AZ31 and its MAO coating, respectively; the round morphologies of cells on the MAO coating was because the micro-pores/cracks on the rough surface exerted stronger constraints on the spreading of cells.

(4) MAO coating showed better cell viability as compared with the Mg substrate, which was related to the higher specific surface area. Results implied that the MAO coating on Mg alloy greatly improved its cytocompatibility.

CRediT authorship contribution statement

Zhao-Qi Zhang: Conceptualization, Writing - original draft, Investigation, Validation. **Li Wang:** Project administration, Software. **Mei-Qi Zeng:** Data curation, Formal analysis. **Rong-Chang Zeng:** Funding acquisition, Writing - review & editing, Methodology, Visualization. **M. Bobby Kannan:** Writing - review & editing. **Cun-Guo Lin:** Resources, Supervision. **Yu-Feng Zheng:** Writing - review & editing.

Declaration of competing interest

The authors declare that they have no known competing financial interests or personal relationships that could have appeared to influence the work reported in this paper.

Acknowledgement

This work was supported by the National Natural Science Foundation of China (51571134) and the SDUST Research Fund (2014TDJH104).

References

[1] L.Y. Li, B. Liu, R.C. Zeng, S.Q. Li, F. Zhang, Y.H. Zou, H.G. Jiang, X.B. Chen, S.K. Guan, Q.Y. Liu, In vitro corrosion of magnesium alloy AZ31 — a synergetic influence of glucose and tris, Front. Mater. Sci. 12 (2018) 184–197.
[2] M.B. Kannan, A. Yamamoto, H. Khakbaz, Influence of living cells (L929) on the biodegradation of magnesium-calcium alloy, Colloids Surf., B 126 (2015) 603–606.
[3] Y.C. Zhao, M.C. Zhao, R. Xu, L. Liu, J.X. Tao, C. Gao, C. Shuai, A. Atrens, Formation and characteristic corrosion behavior of alternately lamellar arranged α and β in as-cast AZ91 Mg alloy, J. Alloys Compd. 770 (2019) 549–558.
[4] M. Wolff, M. Luczak, J.G. Schaper, B. Wiese, M. Dahms, T. Ebel, R. Willumeit-Romer, T. Klassen, In vitro biodegradation testing of Mg-alloy EZK400 and manufacturing of implant prototypes using PM (powder metallurgy) methods, Bioact. Mater. 3 (2018) 213–217.
[5] I.P. Etim, W. Zhang, L. Tan, K. Yang, Influence of stamping on the biodegradation behavior of Mg–2Zn-0.5Nd (ZN20) sheet, Bioact. Mater. 5 (2020) 133–141.
[6] L.Y. Cui, X.T. Li, R.C. Zeng, S.Q. Li, E.H. Han, L. Song, In vitro corrosion of Mg–Ca alloy — the influence of glucose content, Front. Mater. Sci. 11 (2017) 284–295.
[7] R. Karunakaran, S. Ortgies, A. Tamayol, F. Bobaru, M.P. Sealy, Additive manufacturing of magnesium alloys, Bioact. Mater. 5 (2020) 44–54.
[8] G. Zhang, L. Wu, A. Tang, Y. Ma, G.L. Song, D. Zheng, B. Jiang, A. Atrens, F. Pan, Active corrosion protection by a smart coating based on a MgAl-layered double hydroxide on a cerium-modified plasma electrolytic oxidation coating on Mg alloy AZ31, Corrosion Sci. 139 (2018) 370–382.
[9] G. Zhang, L. Wu, A. Tang, X.-B. Chen, Y. Ma, Y. Long, P. Peng, X. Ding, H. Pan, F. Pan, Growth behavior of MgAl-layered double hydroxide films by conversion of anodic films on magnesium alloy AZ31 and their corrosion protection, Appl. Surf. Sci. 456 (2018) 419–429.
[10] M.B. Kannan, O. Wallipa, Potentiostatic pulse-deposition of calcium phosphate on magnesium alloy for temporary implant applications–an in vitro corrosion study,

Mater. Sci. Eng. C 33 (2013) 675–679.
[11] M.B. Kannan, Electrochemical deposition of calcium phosphates on magnesium and its alloys for improved biodegradation performance: a review, Surf. Coating. Technol. 301 (2016) 36–41.
[12] P. Liu, J.M. Wang, X.T. Yu, X.B. Chen, S.Q. Li, D.C. Chen, S.K. Guan, R.C. Zeng, L.Y. Cui, Corrosion resistance of bioinspired DNA-induced Ca–P coating on biodegradable magnesium alloy, J. Magnes. Alloys 7 (2019) 144–154.
[13] Y.H. Zou, J. Wang, L.Y. Cui, R.C. Zeng, Q.Z. Wang, Q.X. Han, J. Qiu, X.B. Chen, D.C. Chen, S.K. Guan, Y.F. Zheng, Corrosion resistance and antibacterial activity of zinc-loaded montmorillonite coatings on biodegradable magnesium alloy AZ31, Acta Biomater. 98 (2019) 196–214.
[14] A. Alabbasi, S. Liyanaarachchi, M.B. Kannan, Polylactic acid coating on a biodegradable magnesium alloy: an in vitro degradation study by electrochemical impedance spectroscopy, Thin Solid Films 520 (2012) 6841–6844.
[15] X. Yan, M.C. Zhao, Y. Yang, L. Tan, Y.C. Zhao, D.F. Yin, K. Yang, A. Atrens, Improvement of biodegradable and antibacterial properties by solution treatment and micro-arc oxidation (MAO) of a magnesium alloy with a trace of copper, Corrosion Sci. 156 (2019) 125–138.
[16] C.Y. Li, C. Yu, R.C. Zeng, B.C. Zhang, L.Y. Cui, J. Wan, Y. Xia, In vitro corrosion resistance of a Ta2O5 nanofilm on MAO coated magnesium alloy AZ31 by atomic layer deposition, Bioact. Mater. 5 (2020) 34–43.
[17] L.Y. Cui, X.H. Fang, W. Cao, R.C. Zeng, S.Q. Li, X.B. Chen, Y.H. Zou, S.K. Guan, E.H. Han, In vitro corrosion resistance of a layer-by-layer assembled DNA coating on magnesium alloy, Appl. Surf. Sci. 457 (2018) 49–58.
[18] L.Y. Cui, P.H. Qin, X.L. Huang, Z.Z. Yin, R.C. Zeng, S.Q. Li, E.H. Han, Z.L. Wang, Electrodeposition of TiO 2 layer-by-layer assembled composite coating and silane treatment on Mg alloy for corrosion resistance, Surf. Coating. Technol. 324 (2017) 560–568.
[19] R. Zeng, L. Cui, K. Jiang, R. Liu, B. Zhao, Y. Zheng, In vitro corrosion and cytocompatibility of a microarc oxidation coating and poly(L-Lactic acid) composite coating on Mg-1Li-1Ca alloy for orthopaedic implants, ACS Appl. Mater. Interfaces 8 (2016) 10014–10028.
[20] M. Badar, H. Lunsdorf, F. Evertz, M.I. Rahim, B. Glasmacher, H. Hauser, P.P. Mueller, The formation of an organic coat and the release of corrosion microparticles from metallic magnesium implants, Acta Biomater. 9 (2013) 7580–7589.
[21] A. Carangelo, A. Acquesta, T. Monetta, Durability of AZ31 magnesium biodegradable alloys polydopamine aided. Part 2: ageing in Hank's solution, J. Magnes. Alloys 7 (2019) 218–226.
[22] V. Dehnavi, W.J. Binns, J.J. Noël, D.W. Shoesmith, B.L. Luan, Growth behaviour of low-energy plasma electrolytic oxidation coatings on a magnesium alloy, J. Magnes. Alloys 6 (2018) 229–237.
[23] Y. Wang, D. Wei, J. Yu, S. Di, Effects of Al2O3 nano-additive on performance of micro-arc oxidation coatings formed on AZ91D Mg alloy, J. Mater. Sci. Technol. 30 (2014) 984–990.
[24] Y. Yang, H. Wu, Effects of current frequency on the microstructure and wear resistance of ceramic coatings embedded with SiC nano-particles produced by microarc oxidation on AZ91D magnesium alloy, J. Mater. Sci. Technol. 26 (2010) 865–871.
[25] M.S. Song, R.C. Zeng, Y.F. Ding, R.W. Li, M. Easton, I. Cole, N. Birbilis, X.B. Chen, Recent advances in biodegradation controls over Mg alloys for bone fracture management: a review, J. Mater. Sci. Technol. 35 (2019) 535–544.
[26] X.N. Gu, N. Li, W.R. Zhou, Y.F. Zheng, X. Zhao, Q.Z. Cai, L. Ruan, Corrosion resistance and surface biocompatibility of a microarc oxidation coating on a Mg-Ca alloy, Acta Biomater. 7 (2011) 1880–1889.
[27] Z. Yao, L. Li, Z. Jiang, Adjustment of the ratio of Ca/P in the ceramic coating on Mg alloy by plasma electrolytic oxidation, Appl. Surf. Sci. 255 (2009) 6724–6728.
[28] J.L. Xu, F. Liu, F.P. Wang, D.Z. Yu, L.C. Zhao, Microstructure and corrosion resistance behavior of ceramic coatings on biomedical NiTi alloy prepared by microarc oxidation, Appl. Surf. Sci. 254 (2008) 6642–6647.
[29] Z.Z. Yin, W.C. Qi, R.C. Zeng, X.B. Chen, C.D. Gu, S.K. Guan, Y.F. Zheng, Advances in coatings on biodegradable magnesium alloys, J. Magnes. Alloysdoi.org/10.1016/j.jma.2019.09.008.
[30] X. Jiang, A. Yu, Silver nanoplates: a highly sensitive material toward inorganic anions, Langmuir 24 (2008) 4300–4309.
[31] R.C. Zeng, X.T. Li, S.Q. Li, F. Zhang, E.H. Han, In vitro degradation of pure Mg in response to glucose, Sci. Rep. 5 (2015) 13026.
[32] Y. Wang, L.Y. Cui, R.C. Zeng, S.Q. Li, Y.H. Zou, E.H. Han, In vitro degradation of pure magnesium-the effects of glucose and/or amino acid, Materials 10 (2017) 725.
[33] C.L. Liu, Y.J. Wang, R.C. Zeng, X.M. Zhang, W.J. Huang, P.K. Chu, In vitro corrosion degradation behaviour of Mg–Ca alloy in the presence of albumin, Corrosion Sci. 52 (2010) 3341–3347.
[34] A. Yamamoto, S. Hiromoto, Effect of inorganic salts, amino acids and proteins on the degradation of pure magnesium in vitro, Mater. Sci. Eng. C 29 (2009) 1559–1568.
[35] Y. Wang, C.S. Lim, C.V. Lim, M.S. Yong, E.K. Teo, L.N. Moh, In vitro degradation behavior of M1A magnesium alloy in protein-containing simulated body fluid, Mater. Sci. Eng. C 31 (2011) 579–587.
[36] C.Y. Li, X.L. Fan, R.C. Zeng, L.Y. Cui, S.Q. Li, F. Zhang, Q.K. He, M.B. Kannan, H.W.G. Jiang, D.C. Chen, S.K. Guan, Corrosion resistance of in-situ growth of nano-sized $Mg(OH)_2$ on micro-arc oxidized magnesium alloy AZ3I influence of EDTA, J. Mater. Sci. Technol. 35 (2019) 1088–1098.
[37] L.Y. Cui, S.D. Gao, P.P. Li, R.C. Zeng, F. Zhang, S.Q. Li, E.H. Han, Corrosion resistance of a self-healing micro-arc oxidation/polymethyltrimethoxysilane composite coating on magnesium alloy AZ31, Corrosion Sci. 118 (2017) 84–95.
[38] Z. Shi, A. Atrens, An innovative specimen configuration for the study of Mg corrosion, Corrosion Sci. 53 (2011) 226–246.
[39] N. Hara, Y. Kobayashi, D. Kagaya, N. Akao, Formation and breakdown of surface films on magnesium and its alloys in aqueous solutions, Corrosion Sci. 49 (2007) 166–175.
[40] G.L. Song, A. Atrens, Corrosion mechanisms of magnesium alloys, Adv. Eng. Mater. 1 (1999) 11–33.
[41] C.L. Liu, Y. Zhang, C.Y. Zhang, W. Wang, W.J. Huang, P.K. Chu, Synergistic effect of chloride ion and albumin on the corrosion of pure magnesium, Front. Mater. Sci. 8 (2014) 244–255.
[42] N. Padilla, A. Bronson, Electrochemical characterization of albumin protein on Ti-6AL-4V alloy immersed in a simulated plasma solution, J. Biomed. Mater. Res. 81 (2007) 531–543.
[43] R. Rettig, S. Virtanen, Time-dependent electrochemical characterization of the corrosion of a magnesium rare-earth alloy in simulated body fluids, J. Biomed. Mater. Res. 85 (2008) 167–175.
[44] M.B. Kannan, R. Walter, A. Yamamoto, Biocompatibility and in vitro degradation behavior of magnesium–calcium alloy coated with calcium phosphate using an unconventional electrolyte, ACS Biomater. Sci. Eng. 2 (2015) 56–64.
[45] Y. Feng, X. Ma, L. Chang, S. Zhu, S. Guan, Characterization and cytocompatibility of polydopamine on MAO-HA coating supported on Mg-Zn-Ca alloy, Surf. Interface Anal. 49 (2017) 1115–1123.
[46] A. Klinger, D. Steinberg, D. Kohavi, M.N. Sela, Mechanism of adsorption of human albumin to titanium in vitro, J. Biomed. Mater. Res. 36 (1997) 387–392.
[47] T. Li, Y. He, J. Zhou, S. Tang, Y. Yang, X. Wang, Influence of albumin on in vitro degradation behavior of biodegradable Mg-1.5Zn-0.6Zr-0.2Sc alloy, Mater. Lett. 217 (2018) 227–230.
[48] C. Liu, Y. Xin, X. Tian, P.K. Chu, Degradation susceptibility of surgical magnesium alloy in artificial biological fluid containing albumin, J. Mater. Res. 22 (2011) 1806–1814.
[49] F. Gong, J. Shen, R. Gao, X. Xiong, L. Xiong, Enhanced corrosion resistance of magnesium alloy by a silane-based solution treatment after an in-situ formation of the $Mg(OH)_2$ layer, Appl. Surf. Sci. 365 (2016) S0169433216000428.
[50] Y. Ren, E. Babaie, S.B. Bhaduri, Nanostructured amorphous magnesium phosphate/poly (lactic acid) composite coating for enhanced corrosion resistance and bioactivity of biodegradable AZ31 magnesium alloy, Prog. Org. Coating 118 (2018) 1–8.
[51] T.S. Lim, H.S. Ryu, S.H. Hong, Electrochemical corrosion properties of CeO_2-containing coatings on AZ31 magnesium alloys prepared by plasma electrolytic oxidation, Corrosion Sci. 62 (2012) 104–111.
[52] P. Wan, X. Lin, L.L. Tan, L.G. Li, W.R. Li, K. Yang, Influence of albumin and inorganic ions on electrochemical corrosion behavior of plasma electrolytic oxidation coated magnesium for surgical implants, Appl. Surf. Sci. 282 (2013) 186–194.
[53] L. Liu, Y. Meng, A.A. Volinsky, H.J. Zhang, L.N. Wang, Influences of albumin on in vitro corrosion of pure Zn in artificial plasma, Corrosion Sci. 153 (2019) 341–356.
[54] X. Ma, S. Zhu, L. Wang, C. Ji, C. Ren, S. Guan, Synthesis and properties of a biocomposite coating formed on magnesium alloy by one-step method of micro-arc oxidation, J. Alloys Compd. 590 (2014) 247–253.
[55] K.K. Kaysinger, W.K. Ramp, Extracellular pH modulates the activity of cultured human osteoblasts, J. Cell. Biochem. 68 (1998) 83–89.
[56] F. Deng, W. Zhang, P. Zhang, C. Liu, J. Ling, Improvement in the morphology of micro-arc oxidised titanium surfaces: a new process to increase osteoblast response, Mater. Sci. Eng. C 30 (2010) 141–147.
[57] L.H. Li, H.W. Kim, S.H. Lee, Y.M. Kong, H.E. Kim, Biocompatibility of titanium implants modified by microarc oxidation and hydroxyapatite coating, J. Biomed. Mater. Res. 73 (2005) 48–54.
[58] Q. Zong, L. Wang, S. Wen, G. Liu, Active deposition of bis (8-hydroxyquinoline) magnesium coating for enhanced corrosion resistance of AZ91D alloy, Corrosion Sci. 89 (2014) 127–136.
[59] G.S. Frankel, A. Samaniego, N. Birbilis, Evolution of hydrogen at dissolving magnesium surfaces, Corrosion Sci. 70 (2013) 104–111.
[60] S. Thomas, N.V. Medhekar, G.S. Frankel, N. Birbilis, Corrosion mechanism and hydrogen evolution on Mg, Curr. Opin. Solid State Mater. Sci. 19 (2015) 85–94.
[61] W.D. Mueller, M.F. de Mele, M.L. Nascimento, M. Zeddies, Degradation of magnesium and its alloys: dependence on the composition of the synthetic biological media, J. Biomed. Mater. Res. 90 (2009) 487–495.
[62] F. El-Taib Heakal, A.M. Bakry, Serum albumin can influence magnesium alloy degradation in simulated blood plasma for cardiovascular stenting, Mater. Chem. Phys. 220 (2018) 35–49.
[63] L.Y. Cui, R.C. Zeng, S.K. Guan, W.C. Qi, F. Zhang, S.Q. Li, E.H. Han, Degradation mechanism of micro-arc oxidation coatings on biodegradable Mg-Ca alloys: the influence of porosity, J. Alloys Compd. (2017) 2464–2476.
[64] G.A. Parks, The isoelectric points of solid oxides, solid hydroxides, and aqueous hydroxo complex systems, Chem. Rev. 65 (1965) 177–198.
[65] K. Kubo, N. Tsukimura, F. Iwasa, T. Ueno, L. Saruwatari, H. Aita, W.A. Chiou, T. Ogawa, Cellular behavior on TiO_2 nanonodular structures in a micro-to-nanoscale hierarchy model, Biomaterials 30 (2009) 5319–5329.
[66] J.I. Rosales Leal, M.A. Rodríguez Valverde, G. Mazzaglia, P.J. Ramón Torregrosa, L. Díaz Rodríguez, O. García-Martínez, M. Vallecillo Capilla, C. Ruiz, M.A. Cabrerizo Vílchez, Effect of roughness, wettability and morphology of engineered titanium surfaces on osteoblast-like cell adhesion, Colloids Surf., A 365 (2010) 222–229.
[67] C. Wu, M. Chen, T. Zheng, X. Yang, Effect of surface roughness on the initial response of MC3T3-E1 cells cultured on polished titanium alloy, Bio Med. Mater. Eng. 26 (2015) S155–S164.